Full Text View

Volume 30, Issue 10 (October 2000)

Journal of Physical Oceanography
Article: pp. 2627–2635 | Abstract | PDF (713K)

Horizontal and Vertical Structure of the Representer Functions for Sea Surface Measurements in a Coastal Circulation Model

Vincent Echevin* **and Pierre De Mey**

LEGOS/GRGS, Toulouse, France

Geir Evensen

Nansen Environmental and Remote Sensing Center, Bergen, Norway

(Manuscript received December 11, 1998, in final form November 29, 1999)

DOI: 10.1175/1520-0485(2000)030<2627:HAVSOT>2.0.CO;2

ABSTRACT

The representer functions used to propagate the information from observations onto model variables in a sequential data assimilation scheme are calculated with a statistical method. The Princeton Ocean Model is used in a simple configuration simulating the North Current flowing along the French coasts in the northwestern Mediterranean Sea. The influence of sea level measurements on the models' three-dimensional temperature and velocity fields is investigated. Inhomogeneities and directions of anisotropy are evidenced. A comparison with simplified reduced order assimilation methods suggests that such schemes will not allow for consistent assimilation of nearshore altimetric data.

1. Introduction

The data assimilation problem for the circulation in coastal regions is often much more complex than what one finds for the larger-scale open ocean circulation. The coastal circulation is strongly influenced by local bathymetry and coastlines, and includes several physical processes such as the wind-driven circulation, tides, storm surges, and shelf waves. Nonlinear processes play a more important role in coastal dynamics than for open ocean circulation. Further, the short temporal and spatial scales involved in these processes means that the relative density of in situ and space-borne measurements will be lower than what one have in the open ocean.

Nevertheless, it is important to describe the coastal ocean circulation with a great accuracy for potential ecological and economical purposes. To reach this goal data assimilation methods which combine optimally observations and model predictions can be very helpful.

Numerous data assimilation methods have been developed for studies of the open ocean mesoscale circulation (see, e.g., De Mey 1997) along with the advancement of satellite altimetry (*ERS-1/2,* TOPEX/Poseidon, Jason Project). At the scale of a few hundred kilometers, the temporal sampling of altimetric satellites (~ 10 days for TOPEX/Poseidon) is sufficient to observe the mesoscale eddy field. Most of the routinely used methods make some simple assumptions: they decouple the problem in the vertical and the horizontal. The surface information is projected in the vertical following some physical and/or statistical principles (De Mey et al. 2000, hereafter DBA; Gavart and De Mey 1997; Cooper and Haines 1996). In the horizontal the extrapolation of the surface information on the model grid is generally done using analytical functions with specified decorrelation scales.

In the coastal ocean, the sampling of measurements generally lacks the resolution needed to resolve the short scales of the circulation. In situ measurements arrays are generally confined to a few locations (for instance across the shelf break to capture a coastal current vertical structure) and lack horizontal resolution to give an accurate three-dimensional description of the density field. Altimetry provides a long-term time survey of the open ocean and data are available up to 25 km from the coast. This represents a potential source of information which has not yet been properly exploited for data assimilation applications in coastal areas.

The simple hypothesis used in optimal interpolation (OI) is generally not valid in coastal areas. Covariances may become anisotropic and will dependent strongly on the local physical conditions such as topography and effects of coastlines. To capture the various scales necessary to adequately project information from observations onto the model variables, it is possible to compute the optimal influence functions, or representers as discussed by Bennett (1992), using Monte Carlo methods such as the Ensemble Kalman Filter (ENKF) as was done by Evensen (1994) and Evensen and van Leeuwen (1996). No simplification of the physics is required. Furthermore, the calculation of influence functions does not require the full storage of the forecast error covariance matrix (of size n^2, n being the dimension of the model state). Only of $O(100)$ model states needs to be stored.

The use of better and dynamically consistent influence functions should improve the results from coastal data assimilation systems. It would help both for the sampling problem since more information is correctly extracted from the observations, and dynamically consistent influence functions are used.

In this note we will examine the spatial structure of the influence functions of sea level measurements, as computed from a set of model states. The horizontal and vertical structure of the influence functions will be discussed with emphasis on the effects of coastlines and topography. The analysis increments computed using the statistical method are also compared with those found using traditional OI schemes, which are not dynamically consistent in coastal areas.

2. Methodology

A sequential assimilation scheme consists of optimizing the model state each time that measurements are available by minimizing a penalty function,

$$J(\psi^a) = (\psi^a - \psi^f)^{\mathrm{T}}(\mathbf{P}^f)^{-1}(\psi^a - \psi^f) + (\mathbf{y}^o - \mathbf{H}\psi^a)^{\mathrm{T}}\mathbf{R}^{-1}(\mathbf{y}^o - \mathbf{H}\psi^a), \quad (1)$$

where ψ^a is the analyzed state, ψ^f is the model forecast, $\mathbf{y}^o$ is the data vector, $\mathbf{H}$ is the observation matrix, $\mathbf{P}^f$ is the forecast error covariance matrix, and $\mathbf{R}$ is the observation error covariance matrix.

The analysis ψ^a, minimizing (1), can be written in terms of influence functions as

$$\psi^a = \psi^f + \sum_{j=1}^{m} b_j \mathbf{r}_j, \quad (2)$$

where the vectors $\mathbf{r}_j$ are the columns of the matrix $\mathbf{P}^f\mathbf{H}^{\mathrm{T}}$. The vector of coefficients, $\mathbf{b} = (b_1, \cdots, b_j, \cdots, b_m)^{\mathrm{T}}$, has the same dimension as the measurement vector, $\mathbf{y}^o = (y^o{}_1, \cdots, y^o{}_m)^{\mathrm{T}}$, and satisfies the system $(\mathbf{H}\mathbf{P}^f\mathbf{H}^{\mathrm{T}} + \mathbf{R})\mathbf{b} = (\mathbf{y}^o - \mathbf{H}\psi^f)$.

The first term in (1) may be written $\langle \psi^a - \psi^f, \psi^a - \psi^f \rangle$ where the inner product $\langle \psi, \phi \rangle = \psi^{\mathrm{T}}(\mathbf{P}^f)^{-1}\phi$ defines a Hilbert

space of functions over the "ocean" space. Therefore the $\mathbf{r}_j$ in (2) are the so-called representers uniquely defined by the inner product and the relation $\langle \mathbf{r}_j, \boldsymbol{\psi} \rangle = \mathbf{H}_j \boldsymbol{\psi}$ (Bennett 1992), with $\mathbf{H}_j$ the observation matrix for measurement j. In the present case, the inner product is rather simple and the computation of the representers is straightforward: $\langle \mathbf{r}_j, \boldsymbol{\psi} \rangle = \mathbf{H}_j \boldsymbol{\psi} = \mathbf{r}^{\mathrm{T}}{}_j (\mathbf{P}^f)^{-1} \boldsymbol{\psi}$ thus $\mathbf{r}^{\mathrm{T}}{}_j = \mathbf{H}_j \mathbf{P}^f$. If a more complex inner product were used, involving, say, integrals over a period of time, constraints on the initial conditions (for specific examples, see Bennett 1992), the computation of the representers would require the integration of the so-called adjoint equations.

In the ENKF, the matrix $\mathbf{P}^f \mathbf{H}^{\mathrm{T}}$ is estimated from a set of model states ($\boldsymbol{\psi}^1, \ldots, \boldsymbol{\psi}^N$) representing the probability distribution of $\boldsymbol{\psi}$. The calculation of the representers is simple: for a measurement of sea level η at location $\mathbf{x}_0$, the representer is a vector of correlations between the model variable $\eta(\mathbf{x}_0)$ and all other model variables. For example, the zonal velocity of the analyzed state at location $\mathbf{x}_1$ is $u^a(\mathbf{x}_1)$, with

$$u^a(\mathbf{x}_1) = u^f(\mathbf{x}_1) + b_0 \langle \eta(\mathbf{x}_0), u(\mathbf{x}_1) \rangle. \quad (3)$$

The covariance is calculated from the ensemble of N states,

$$\langle \eta(\mathbf{x}_0), u(\mathbf{x}_1) \rangle = \frac{1}{N-1} \sum_{i=1}^{N} \left[\eta^i(\mathbf{x}_0) - \frac{1}{N} \sum_{k=1}^{N} \eta^k(\mathbf{x}_0) \right] \times \left[u^i(\mathbf{x}_1) - \frac{1}{N} \sum_{k=1}^{N} u^k(\mathbf{x}_1) \right]. \quad (4)$$

In OI schemes, $\mathbf{P}^f$ is generally not estimated from model runs. In some cases, $\mathbf{P}^f$ is decomposed into a product $(\mathbf{D}^f)^{1/2} \mathbf{C} (\mathbf{D}^f)^{1/2}$ where $\mathbf{D}^f$ is the diagonal matrix of variances and $\mathbf{C}$ is a specified covariance matrix that does not evolve in time (De Mey 1997). Moreover there may be a reduction of the physical space: the assimilation is performed in a reduced space, say a two-dimensionnal space spanned by a base of vertical empirical orthogonal functions, and the projection of the analyzed state back in the initial space of the model is based on some physical or statistical hypotheses.

In this study, the representers corresponding to sea surface measurements at different locations in the model domain are calculated with a statistical method. The representer fields are multiplied by the coefficient b_0 that correspond to a model–data misfit $\delta\eta = 5$ cm. The assumed observation error variance is $\sigma = 1$ cm rms, thus $b_0 = \delta\eta(\mathbf{x}_0)/(\langle \eta(\mathbf{x}_0), \eta(\mathbf{x}_0) \rangle + \sigma^2)$.

A set of 150 model states is integrated with the free surface sigma coordinate primitive equations Princeton Ocean Model (POM) model (Blumberg and Mellor 1987) from a set of perturbed initial conditions. The model is run in a simplified setup featuring a baroclinic coastal current flowing along a coast and onto a shelf representing the Gulf of Lions coastal shelf. A spinup run of 40 days with no thermodynamic and wind forcing is performed to establish the circulation. Day 40 is then taken as the initial state from which a set of perturbed initial conditions is generated by displacing vertically the isopycnals. Horizontally and vertically correlated fields of random displacements are generated following Evensen (1994). The horizontal decorrelation scale is 30 km. It corresponds to ~ 2–3 times the first internal Rossby radius in the coastal area. The scales for the vertical displacements are of o(50 m). Each model state is integrated for 10 days before statistics are computed. Within this time period the perturbations are able to trigger instabilities of the coastal current with a variety of scales in agreement with the observations (Crepon et al. 1982). Open boundary conditions, wind and thermodynamic forcing perturbations are not considered in this study.

3. Horizontal structure of the representer functions

The response to the same model–data misfit input ($\delta\eta = 5$ cm) is strongly dependent on the location of the measurement. Four measurement locations are chosen. Two are located in the eastern part of the model domain at approximately 20 and 70 km from the coast (see Figs. 1 and 2). The location at 70 km from the coast corresponds to the axis of the coastal current. In the western part of the domain one measurement is located above the shelf break (Fig. 3), while the other is located just off the shelf at 200-m depth (Fig. 4).

The response to a sea level rise results in the creation of an anticyclonic circulation around the location of the

measurement. There is a geostrophic adjustment to the sea level rise. However, the anticyclonic structure is not necessarily centered at the measurement location as might be expected. For the measurement located closest to the shelf (Fig. 4), the anticyclonic velocity structure is shifted 10–20 km south of the measurement location. The horizontal scales of the velocity structures are different in the eastern and western part of the model domain. In the east (Figs. 1 and 2) the horizontal scale of the anticyclonic structure is shorter than in the western part. The intensity of the velocity correction at 5 m is stronger in the eastern part. The temperature corrections have different intensities dependent of the location. They are stronger in the surface layers in the eastern part than in the western part. The maxima of the temperature corrections are located at varying distances from the measurement sites, sometimes up to 20–30 km as is seen in Fig. 2. There is a negative temperature correction along the north-western part of the anticyclonic structures for all measurements at 5 m, especially in the eastern part (Figs. 1 and 2). This may be due to the southward deviation of the warm coastal current correlated with a local sea level rise.

Anisotropy appears in both the velocity and temperature corrections. The velocity structures are relatively symmetric around measurement sites located far from the coast (Figs. 2 and 3). Near the coast (Fig. 1), the north-western branch of the velocity correction is enhanced between the coast and the measurement site. The temperature gradient of the correction is greater between the coast and the measurement location than south of the measurement location.

4. Vertical cross-shore structure of the representer functions

The vertical and cross-shore structure of the analysis increments can be examined by looking at meridional sections of the corrections fields. Again there are apparent differences between the influences from the observations at the different locations. The temperature and velocity corrections closest to the shelf show a strong influence of the topography (Fig. 6). The influence of the measurement spreads towards deeper areas south of the shelf. This results in a strong anisotropy in the velocity correction, with a maximum at 100 m above the slope. For measurements in the western part the correlation of sea surface measurements with the upper ocean temperature is low. It is stronger in the western part of the domain especially for the measurement located near the coast (Fig. 5). There are two local maxima in the temperature correction, one near the surface and one at about 100-m depth. The maximum correction near the surface is probably related to the influence of the warm surface waters of the coastal current.

5. Discussion

An intercomparison of the ensemble based analysis has been made with two standard OI schemes. In these OI schemes used in mesoscale circulation studies, two-dimensional maps of sea surface height anomalies are assimilated into the ocean model. Along-track data are collected during a given time period and then interpolated onto the model grid with some spatial and temporal decorrelation scales. The two-dimensional model–data misfit field is then projected in the vertical based on some “simplified” principles. Examples are the vertical displacement method by Cooper and Haines (1996) where the water column is lifted or lowered to conserve large scale potential vorticity, the projection on the vertical empirical orthogonal modes as was done by DBA and Gavart (1997), or the use of vertical correlations computed from a climatological model run (Mellor and Ezer 1991).

None of these methods takes into account the horizontal anisotropies and asymmetries evidenced with the ensemble method. Moreover, the correction is applied on the tracers and a geostrophic correction is calculated for the velocities. The influence of the data on ageostrophic processes can not be taken into account with these methods, and most of them assume a decoupling between the mixed layer and the deeper ocean. The tracers are corrected only below the mixed layer. Despite the simplicity of the current experiment there are clear evidence of correlations with surface variables, in particular when the observation is located close to the coast (Figs. 5 and 6).

To illustrate the difference between the ENKF and OI, the temperature and velocity corrections have been calculated at the four selected locations using both the method by Cooper and Haines (1996, hereafter CP) and the ENKF.

The CP correction displaces the water column vertically to adjust the surface pressure, given a level of reference (1000 m in our case). For a measured sea level rise this induces a downward translation of the water column located below the mixed layer. In our case the magnitude of the CP correction on temperature in the eastern part of the domain is similar to that of the ENKF correction below 150 m but it is greater by 0.5°C above 150 m (not shown). The negative temperature correction in the surface layers is absent as the upper layers are unchanged in the CP method. The use of an isotropic horizontal correlation scale to interpolate the model–data misfit around the measurement location fails to retrieve the asymmetry in the density correction. As a result the geostrophic correction is symmetric around the location site, contrary to the ENKF correction, which is stronger near the coast. Furthermore, the use of the CP method is limited to deep waters as a level of reference can not be inferred in shallow areas.

The one-dimensional (1D) method consists in using vertical EOFs to calculate a density correction $\delta\rho(\mathbf{x}_0, z)$ located

under the sea level measurement location $\mathbf{x}_0$. The EOFs may be calculated from a data climatology (Gavart and De Mey 1997) or from a set of model runs (DBA). The density correction is then extrapolated horizontally given a specified decorrelation scale r_h. The correction in the vicinity of the measurement is simply

$$\delta\rho(\mathbf{x}, z) = \delta\rho(\mathbf{x}_0, z) \exp\left[-\frac{1}{2}\left(\frac{d(x, x_0)}{r_h}\right)^2\right]. \qquad (5)$$

To evaluate the difference between the ENKF and the 1D method, let us assume that we are able to calculate a correction $\delta\rho(\mathbf{x}_0, z)$ using vertical EOFs under the measurement location $\mathbf{x}_0$. To simplify the problem we do not actually calculate EOFs from a dataset and we assume that the density correction $\delta\rho(\mathbf{x}_0, z)$ under the measurement location $\mathbf{x}_0$ is identical to that of the ENKF method. The correction is then extrapolated horizontally with a specified scale of 25 km as in the 1D method, rather than with the anisotropic horizontal scales computed from the set of model states (ENKF method). In deep areas and far from the coast the produced 1D temperature and geostrophic velocity corrections are close to the ENKF ones (Fig. 7). Near the coast the corrections are different from the ENKF (not shown) since horizontal correlations are isotropic. Near the shelf the 1D method is clearly not valid as anisotropy is stronger (Fig. 4). Consequently the velocity correction is much weaker than the ENKF (Fig. 7).

To test the efficiency of the statistical method, we have performed a simple twin experiment in which the ENKF and the CP methods are compared. We have not implemented the 1D method as it necessitates to calculate vertical EOFs from a data base, which would be inconsistent with the simplicity of the current academic experiment. In the following experiment a simulation was randomly chosen from the set of model runs. It is supposed to represent the "true" state of the ocean which we intend to get close to with the assimilation process. Sea level data are extracted from the "true" state of the ocean. We assumed that an altimetric track was parallel to the y axis at x = 160 km. Twelve data points distant from 15 km were extracted simultaneously along the track. Next, 1-cm sigma squared noise was added to the data. Then this data was compared to the background state and a model–data misfit was computed. In the ENKF method, a model–data misfit and the corresponding analysis (2) are computed for each model run. The best estimate is the mean of the set of analyses. In the CP method, the model–data misfit is computed with a chosen background state (to be consistent we chose the background state as equal to the mean state of the set of model runs before the analyses). Then the model–data misfit is interpolated on the horizontal model grid with an optimal interpolation scheme using a 20 km decorrelation scale. In a last step the vertical displacement of the water column and a geostrophic correction are calculated.

Horizontal sections of the temperature and velocity fields at 50 m for the different solutions are shown in Fig. 8. The coastal current in the background state (bottom left, Fig. 8) is located around the $y \simeq$ 150-km position, whereas it is located around $y \simeq$ 120 km in the true state ("truth"). Note the different scales for the velocity due to smoothing in the computed mean background state. The ENKF solution shows a displacement of the current to the south around $y \simeq$ 120 km. It also shows a decrease of the intensity of the current near the coast around ($x \simeq$ 220 km, $y \simeq$ 180 km). The CP analysis produces a southward meander in the current and a cyclonic structure south of the current. The associated temperature field is stronger by 0.2°C compared to the truth. The veering of the coastal current is very abrupt and the adjustment after the analysis may be difficult. One may argue that the scales of the OI must be increased to smooth horizontally the structures introduced by CP. On this point, the strength of the ENKF lies in its ability to calculate its own horizontal and vertical scales for the interpolation. Indeed the ENKF is able to rectify the position of the coastal current (Fig. 8) and to create smaller mesoscale structures when they are located in the vicinity of the altimetric track (not shown). Moreover a level of no motion must be assumed in the CP method. To deal with this problem a mean vertical density profile was used to complete the density profiles when the depth was lower than 1000 m. Then the vertical profiles were displaced vertically in shallow areas as well as in deep areas. Last, the CP method is not able to correct the dynamical fields in the mixed layer unlike the ENKF. Hence the CP solution in the top 30 m is farther from the true state than the ENKF solution (not shown). Eventually, the CP geostrophic velocity correction was calculated on z levels and then reinterpolated on the sigma model grid. This may induce truncation errors in areas of strong topographic slopes during the forward integration of the model after the analysis. By comparison, the ENKF method does not necessitate an interpolation on z levels since all statistics may be calculated on the model grid regardless of its nature.

6. Conclusions

The statistical method provides an efficient means to calculate the representer functions that propagate the information from observations on model variables, without any simplification of the model dynamics. The representer functions for selected sea level measurements of altimetric type are calculated. Their horizontal and vertical structures show strong anisotropic directions due to the influence of the coastline boundary and topography. Comparison with some reduced order methods which consist in projecting the information vertically to correct the water column show that they may be valid at distances greater than 50 km from the coast in deep areas and far from the shelf break influence. Near the coast the use of the statistical method is efficient to capture the three-dimensional anisotropies. A simple twin experiment was performed to

compare the statistical method to the Cooper and Haines (CP) method. Both schemes are able to displace southward the current, consistently with the true state. Nevertheless the ENKF analysis is more consistent with the coastal dynamics and allows corrections in the surface layers unlike the CP method.

REFERENCES

Bennett, A. F., 1992: *Inverse Methods in Physical Oceanography*. Cambridge University Press, 346 pp..

Blumberg, A. F., and G. L. Mellor, 1987: A description of a three-dimensional coastal ocean circulation model. *Three-Dimensional Coastal Ocean Models*, N. Heaps, Ed., American Geophysical Union, 1–16..

Cooper, M., and K. Haines, 1996: Altimetric assimilation with water property conservation. *J. Geophys. Res.*, **101,** 1059–1077..

Crepon M., L. Wald, and J. M. Longuet, 1982: Low-frequency waves in the Ligurian Sea during December 1997. *J. Geophys. Res.*, **87,** 595–600..

De Mey, P., 1997: Data assimilation at the oceanic mesoscale: A review. *J. Meteor. Soc. Japan*, **75,** 415–427..

— , and M. Benkiran, 2000: A multivariate reduced-order optimal interpolation method and its application to the Mediterranean Basin–scale circulation. *Ocean Forecasting, Conceptual Basis and Applications*, N. Pinardi, Ed., Springer-Verlag, in press..

Evensen, G., 1994: Sequential data assimilation with a nonlinear quasi-geostrophic model using Monte Carlo methods to forecast error statistics. *J. Geophys. Res.*, **99** (C5), 10 143–10 162..

— , and P. J. van Leeuwen, 1996: Assimilation of Geosat altimeter data for the Agulhas Current using the ensemble Kalman filter with a quasigeostrophic model. *Mon. Wea. Rev.*, **124,** 85–96.. Find this article online

Gavart, M., and P. De Mey, 1997: Isopycnal EOFs in the Azores Current region: A statistical tool for dynamical analysis and data assimilation. *J. Phys. Oceanogr.*, **27,** 2146–2157.. Find this article online

Mellor, G. L., and T. Ezer, 1991: A Gulf Stream model and an altimetry assimilation scheme. *J. Geophys. Res.*, **96,** 8779–8795..

Figures

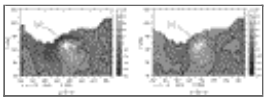

Click on thumbnail for full-sized image.

Fig. 1. Horizontal section at (left) 5-m depth and (right) 50 m of the temperature and velocity corrections in response to a 5 cm model–data sea level misfit at location (a) (x = 340 km, y = 140 km). The surface measurement location is indicated by a small dark square on the left panel. The velocity scale is indicated below the left panel. Units: cm s^{-1}, °C. Negative temperature corrections contours are dark and dotted

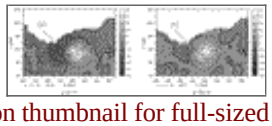

Click on thumbnail for full-sized image.

Fig. 2. Same as Fig. 1 but for a measurement located at (b) (x = 350 km, y = 100 km)

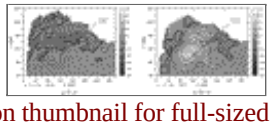

Click on thumbnail for full-sized image.

Fig. 3. Same as Fig. 1 but for a measurement located at (d) (x = 120 km, y = 100 km)

Click on thumbnail for full-sized image.

Fig. 4. Same as Fig. 2 but for a measurement located at (c) (x = 110 km, y = 160 km)

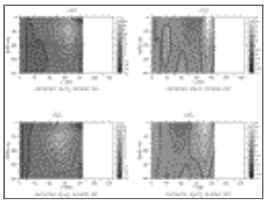

Click on thumbnail for full-sized image.

Fig. 5. Meridional section of the (left) temperature and (right) zonal velocity corrections for sea level measurements located at (a) (upper panels) and (b) (lower panels). The sea level measurement location is indicated by a small dark square located under figure labels (a) and (b)

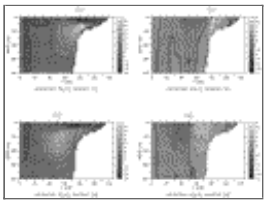

Click on thumbnail for full-sized image.

Fig. 6. Same as Fig. 5 for sea level measurements located at (c) (upper panels) and (d) (lower panels)

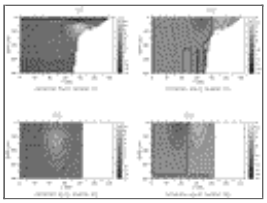

Click on thumbnail for full-sized image.

Fig. 7. Same as Fig. 6 but the density corrections under the measurement are extrapolated with an homogeneous horizontal scale of 25 km. Geostrophic velocity corrections are calculated following $\delta\mathbf{u} = (1/\rho_0 f)\mathbf{k} \times \nabla\mathbf{P}'$

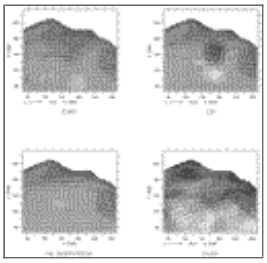

Click on thumbnail for full-sized image.

Fig. 8. Comparison of the ENKF and CP analyzed states with the true state. The temperature and velocity fields at 50-m depth are represented. The scale of the velocity is indicated below each panel and units are cm s^{-1}. Dark shaded areas indicate warm waters (20°C maximum). The isocontours are 0.2°C. The ENKF analyzed state (top left), the background state (bottom left), the CP analyzed state (top right) and the true state (bottom right) are shown

* Current affiliation: LODYC, Paris, France.

Corresponding author address: Dr. Vincent Echevin, LODYC, UPMC, T26, 4E, 4 Place Jussieu, 75252 Paris, Cedex 05, France.

E-mail: vincent.echevin@lodyc.jussieu.fr